Effects of disorder on the Raman spectra of GaAs/AlAs superlattices

Elisa Molinari
Consiglio Nazionale delle Ricerche (CNR), Istituto "O.M. Corbino," via Cassia 1216, I-00189 Roma, Italy

Stefano Baroni,* Paolo Giannozzi, and Stefano de Gironcoli
Institut Romand de Recherche Numérique en Physique des Matériaux (IRRMA), PHB-Ecublens, CH-1015 Lausanne, Switzerland
(Received 29 July 1991)

The vibrational properties of GaAs/AlAs (001) superlattices are studied theoretically by means of an *ab initio* approach—based on *interatomic* force constants—that allows one to treat the effects of compositional disorder using very large supercells. We find that the experimental Raman spectra in thin samples cannot be explained without taking into account disorder occurring at the interfaces. Moreover, we show that some of the AlAs-like LO modes are extremely sensitive to disorder, and they are therefore suitable for a rather precise characterization of the samples.

I. INTRODUCTION

Phonon investigations of semiconductor superlattices (SL's) have developed rapidly in recent years, particularly for $(GaAs)_n/(AlAs)_n$ (001) SL's.[1] Important advances have been achieved in the understanding of the basic microscopic mechanisms which modify the bulk spectra of the two constituent semiconductors due to layering: folding of acoustical modes and confinement of optical modes are by now well-understood mechanisms that govern light-scattering spectra in these materials.[1] Owing to the large difference between the catonic masses, GaAs and AlAs optic modes occur in different frequency ranges. As a consequence, SL optical vibrations are confined in one or the other material according to their frequencies. Two basic problems still exist in the interpretation of light-scattering data. The first ("problem 1") concerns the relation of confined SL frequencies to the dispersions of the bulk constituents for SL's with "thick" layers ($n > 4$), where the very different behavior observed for GaAs-like and AlAs-like modes is not yet understood theoretically. The second ("problem 2") is related to the thickness dependence of the most intense Raman peak, ω_{LO_1}, in ultrathin (UT) SL's ($n \leq 3$), for which the results of all available calculations are in qualitative disagreement with experiments.

Let us examine first the case of thicker SL's. For perfectly ordered interfaces ("ideal SL"), the relation between the frequency of confined modes and the bulk dispersion has been explained a few years ago.[2-4] The frequencies of successive GaAs-like or AlAs-like confined modes (denoted by $\omega_{LO_m}^{GaAs}$ or $\omega_{LO_m}^{AlAs}$, with $m = 1,\ldots,n$) can be mapped onto the corresponding bulk LO dispersions by an appropriate confinement wave vector $q_m = m\pi/d$, d being the confinement length; $d \simeq (n+1)a/2$ (a is the bulk lattice parameter) is found to be a reasonable choice for SL's with $n > 4$. This relation should allow one to recover the bulk dispersions by "unfolding" the SL Raman frequencies through their effective wave vector. From the theoretical point of view, the soundness of this picture is very well confirmed by comparing accurate *ab initio* bulk dispersions with SL spectra calculated at the same level of accuracy (see Sec. III A below). This "unfolding" procedure was first applied to experimental data by Sood *et al.*[2] and subsequently by other groups.[5,6] A collection of results from Ref. 6 is shown in Fig. 1 together with recent theoretical bulk dispersions, which are believed to be very accurate. In the GaAs-like frequency range, Fig. 1 shows a deviation of the unfolded SL points from the bulk dispersion when approaching the zone boundary: the observed frequencies are slightly but consistently higher than expected for ideal SL's, the amount of the deviations depending on the samples used in the experiments.[2,5,6] In the AlAs-like range most groups do not report the observation of successive confined modes. Several modes in the range 360–400 cm^{-1} are reported in Ref. 6 and assigned to confined AlAs-like frequencies. The disagreement between theoretical predictions for ideal SL's and experiments is dramatic in this case. More

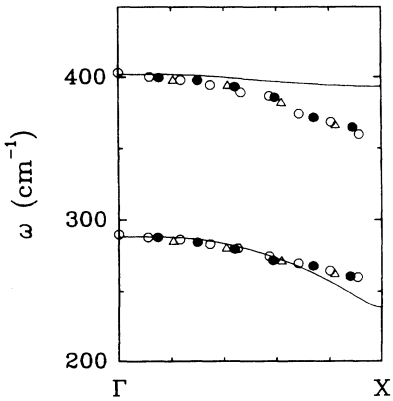

FIG. 1. Frequencies of Raman peaks of GaAs/AlAs (001) superlattices of various thicknesses (symbols as in Ref. 6), "unfolded" onto the theoretical bulk dispersions calculated *ab initio* in Ref. 9 (solid lines: the upper and lower branches correspond to bulk AlAs and GaAs, respectively). The circles at Γ indicate experimental bulk LO frequencies.

recent experiments[7] indicate that the disagreement may be reduced by improving the quality of the samples and by a better characterization of their thickness. However, the mapping of the dispersions is difficult to achieve when approaching the zone boundary, and—when available—it is still unsatisfactory.

The second open question is related to the large discrepancy between theoretical expectations and experiments, which was found for the n dependence of the ω_{LO_1} peaks in ideal UT SL's since the very first studies.[8] This is illustrated in Fig. 2, where we display several sets of experimental data together with the theoretical results of Ref. 9, which are the most accurate so far available.

The above considerations indicate that there are serious difficulties in reconciling the theoretical results for *ideal* SL's with experiments. The purpose of this paper is to show that a proper account of interface disorder can overcome these discrepancies.[10] In Sec. II we present our theoretical framework. In Sec. III we discuss the effect of interfacial disorder on the Raman spectra of GaAs/AlAs SL's. In Sec. IV we present an important byproduct of our investigation: Raman active modes—particularly the AlAs-like ones—turn out to be very sensitive to compositional disorder and they are suitable for a rather precise characterization of the samples. Finally, Sec. V contains our conclusions.

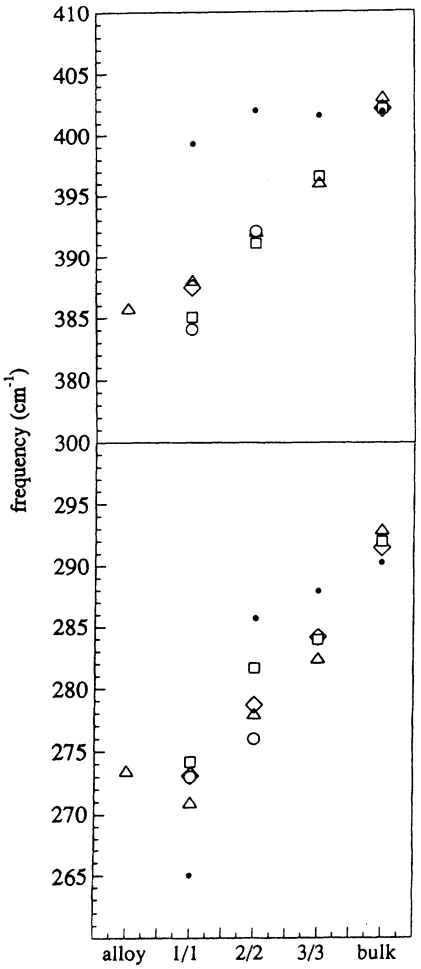

FIG. 2. Collection of GaAs- and AlAs-like LO Raman frequencies measured by several groups for $(\mathrm{GaAs})_n(\mathrm{AlAs})_n$ (001) superlattices. Measured peaks for a random alloy of equivalent composition and for the bulk crystals are also shown for comparison. Diamonds, squares, triangles and circles are from Refs. 8(a)–8(d), respectively. Full dots are the result of *ab initio* calculations for *ideal* superlattices (no cationic intermixing), as in Ref. 9.

II. METHOD

A proper account of cationic intermixing requires the use of large supercells to simulate the effects of disorder. Although the perturbative approach used in our previous investigation[9] is very powerful for large-scale calculations of vibrational spectra, it is still very demanding computationally, and presently limited to systems not larger than ≈ 20 atoms. In the present case of GaAs/AlAs SL's, we use a new scheme which is as simple to use as phenomenological models (thus allowing us to treat systems as large as ≈ 1000 atoms), yet being as accurate and predictive as first-principles calculations. This scheme is described in more detail elsewhere:[11] here we just recall the main underlying ideas.

As a consequence of the close chemical similarity between Ga and Al, the interatomic force constants of GaAs and AlAs are very close to each other, and the force constants of any $\mathrm{Al}_x\mathrm{Ga}_{1-x}\mathrm{As}$ mixed system (superlattice or alloy) are almost independent of composition.[11,12] It is therefore a good approximation to describe the difference between Ga and Al in a mixed $\mathrm{Al}_x\mathrm{Ga}_{1-x}\mathrm{As}$ system just through the different cationic masses ("mass approximation"). To this end, we calculate the *real-space* interatomic force constants to build up the SL dynamical matrix using the appropriate distribution of masses. Phonon frequencies and displacement patterns are then obtained by direct diagonalization of the dynamical matrix. In practice, interatomic force constants C are obtained by Fourier analysis of the dynamical matrices D calculated for the virtual crystal:

$$C_{\alpha i,\beta j}(\mathbf{R}) = \frac{\partial^2 E}{\partial u_{\alpha i}(\mathbf{0})\partial u_{\beta j}(\mathbf{R})} = \frac{\sqrt{M_i M_j}}{N}\sum_{\mathbf{q}} e^{i\mathbf{q}\cdot\mathbf{R}} D_{\alpha i,\beta j}(\mathbf{q}) , \quad (1)$$

where α and β are cartesian indices, i and j indicate atoms in the unit cell, $\mathbf{R}$ is a lattice vector, E is the energy per cell of the system, u's are ionic displacements, M's ionic masses, N the number of unit cells in the crystal, and $\mathbf{q}$ is a wave vector in the Brillouin zone. The dynamical matrices in Eq. (1) are calculated *ab initio* within the density-functional perturbation theory described in Ref. 12, using the same technical ingredients as in Ref. 11. The Fourier transform in Eq. (1) cannot be computed on a discrete grid owing to the nonanalytic character of D at long wavelengths, which is due to the long-range dipole-dipole interactions typical of polar materials. However,

the singular term of the dynamical matrix is *exactly* the same as in a rigid-ion model, provided that the crystal dielectric constant and ionic effective charges are obtained *ab initio* on the same footing as the dynamical matrices. Once the Coulomb term so calculated has been subtracted, D can be Fourier analyzed on a discrete mesh. The size of the reciprocal-space mesh determines the maximum range of the non-Coulomb real-space force constants, $R_{\max}$. The mesh used in the present calculation corresponds to $R_{\max} \sim 2\pi/q_{\min} \sim 3a$. We have verified that beyond this range the (non-Coulomb) force constants vanish for any practical purpose.

The accuracy of the mass approximation—upon which the results of the present paper rely—is demonstrated against fully self-consistent dynamical matrix calculations for the pure GaAs and AlAs materials as well as for a few representative ideal SL's. In Fig. 3 we compare phonon dispersions of GaAs and AlAs, as obtained from accurate self-consistent calculations of the dynamical matrices of GaAs and AlAs independently, and from the mass approximation. The effect of the mass approximation is negligible for acoustic and TO modes, while it is limited to a quasirigid shift of at most 5–6 cm^{-1} towards higher (lower) energies of the GaAs (AlAs)-like LO modes; this shift originates from the slightly over (under)-estimated LO-TO splitting produced for GaAs (AlAs) by the virtual-crystal effective charges. In the following all our results will be affected by such a shift. This is seen clearly in Fig. 4, where we compare the values of ω_{LO_1} for ideally ordered $(\mathrm{GaAs})_n(\mathrm{AlAs})_n$, obtained for various values of n with the mass approximation and via fully self-consistent calculations. In practice, the only effect of the mass approximation is to lower (raise) GaAs (AlAs)-like phonon modes much in the same way as in pure materials. Such a quasirigid shift should be kept in mind when comparing calculated frequencies with experiments.

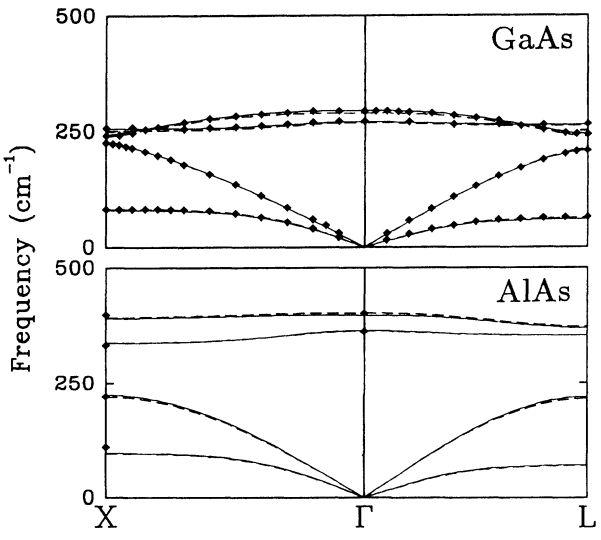

FIG. 3. Phonon dispersion of bulk GaAs and AlAs, obtained by means of full self-consistent calculations (dashed lines) and using virtual crystal interatomic force constants with the mass approximation (solid lines). Symbols represent neutron-scattering experimental data for GaAs (Ref. 21) and the available data from optical experiments for AlAs (Ref. 22).

III. RESULTS

We now present our results for structures with a disordered distribution of cations. As we will see, phonon spectra depend on the cationic arrangement at the interface, which is unknown in practice. We do not aim at reproducing the experimental data in fine detail, but rather at understanding the qualitative mechanisms responsible for the disagreement between previous theoretical predictions and experimental results. Therefore, we concentrate our attention on a few representative cases which will allow us to draw some general conclusions on the role of interfacial disorder on the vibrational properties of these systems. Disorder is treated following the approach described above: intermixed cationic planes are dealt with using tetragonal supercells whose in-plane lattice constant is $3a$, thus containing 18 atoms per two-dimensional unit cell. The total number of atoms con-

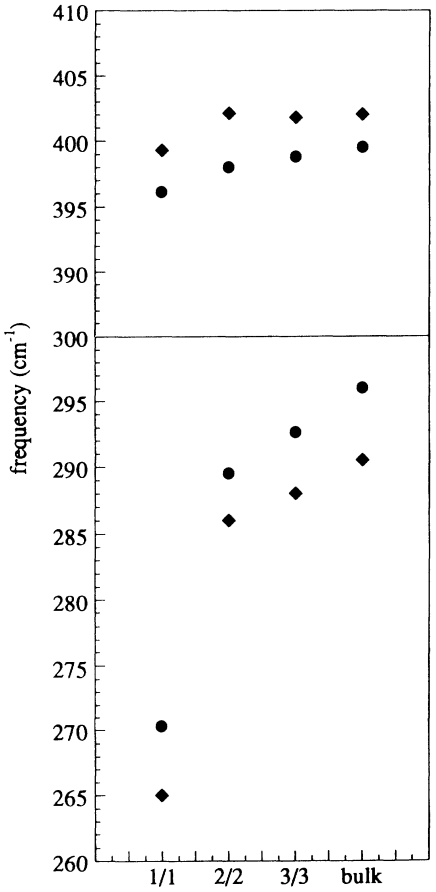

FIG. 4. $\omega_{\mathrm{LO}_1}(\Gamma)$ in ideal $(\mathrm{GaAs})_n(\mathrm{AlAs})_n$ (001) superlattices: comparison between results of full *ab initio* calculations (diamonds, as in Ref. 9) and of calculations based on virtual crystal force constants and the mass approximation (circles).

tained in a supercell for $(GaAs)_n(AlAs)_n$ is, therefore, $4n \times 18$. In the alloyed planes the cationic distribution is chosen at random according to the appropriate concentration, and the calculated properties are averaged over ~ 10 such random configurations.

A. Problem 1: optical SL frequencies vs bulk dispersions

Let us consider as an example the $(GaAs)_5(AlAs)_5$ SL. The calculated[13] $z(xy)\bar{z}$ backscattering Raman spectrum for the ideal SL (no intermixing) is shown in the top panel of Fig. 5(a), and the mode frequencies are plotted by full circles in Fig. 6 versus the appropriate effective wave vectors $q=(m/6)(2\pi/a)$. A comparison with the phonon dispersions for the two independent bulk materials (continuous lines) shows that the picture of LO modes in ideal SL's as confined bulk modes holds to a very high accuracy (the small deviations arise from the residual coupling between successive wells and would disappear for thicker barriers). The failure of this picture to account for some important aspects of the experimental data (as illustrated in Fig. 1) indicates that some kind of disorder must play an important role in the observed spectra.

The simplest example of interfacial disorder can be schematized by the presence of one intermixed cationic layer Al_xGa_{1-x} at each of the two interfaces, which we consider identical for simplicity. The corresponding sequence of atomic layers is

$$(GaAs)_4(Al_xGa_{1-x}As)_1(AlAs)_4(Al_xGa_{1-x}As)_1 .$$

The Raman spectrum is shown in Fig. 5(b) for $x=0.5$, and the peak positions are plotted by open circles in Fig. 6 at the same set of effective q values used for the ideal configuration. The results obtained when two intermixed layers of $Al_{0.5}Ga_{0.5}As$ instead of one are present at the interfaces are displayed by open squares in Fig. 6. A comparison between Figs. 1 and 6 indicates that the oc-

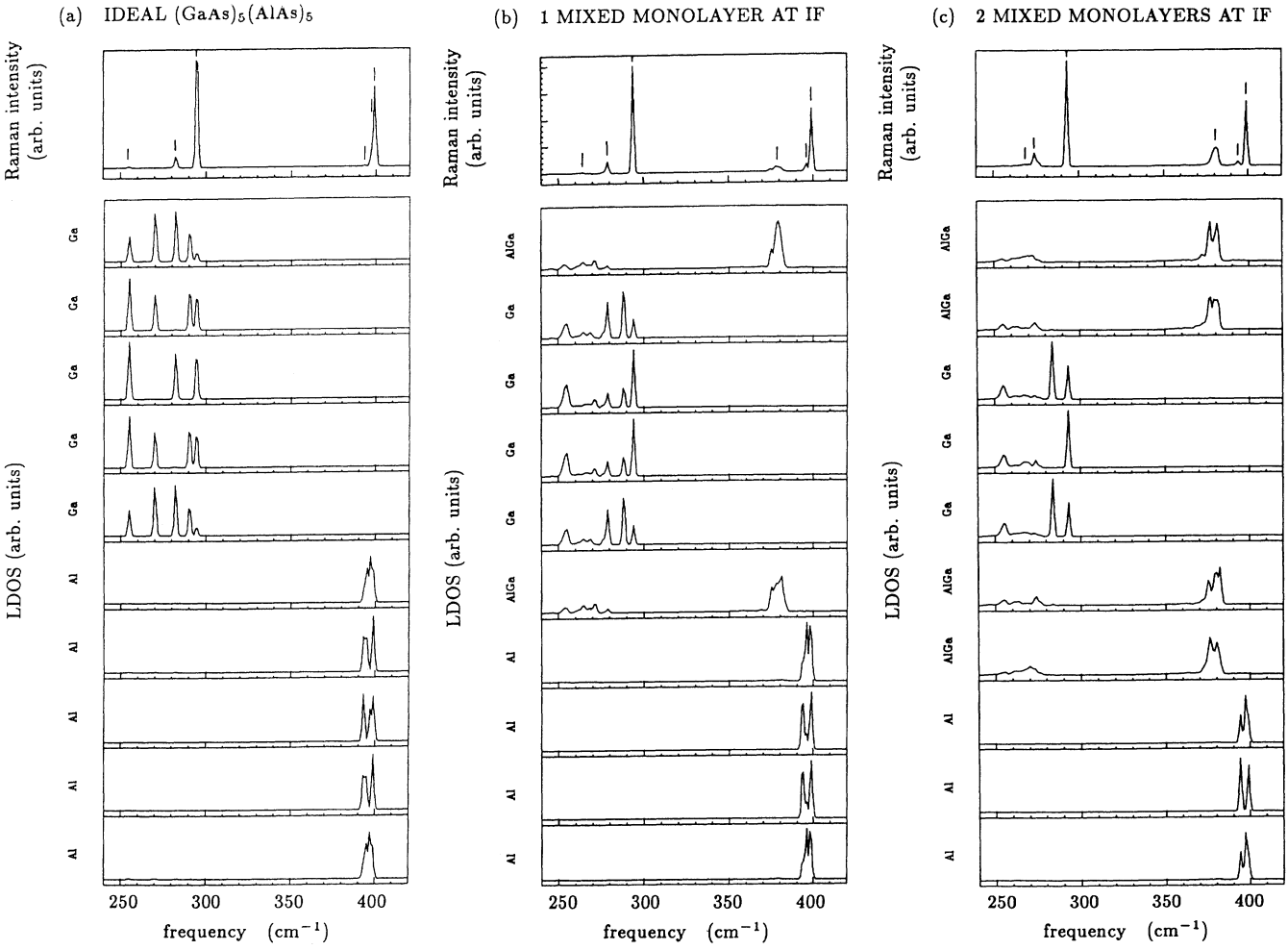

FIG. 5. Top panels: calculated Raman intensity [$z(xy)\bar{z}$ configuration] for the ideal $(GaAs)_5(AlAs)_5$ (001) superlattice (a) and for superlattices with the same periodicity but with one or two intermixed $Al_{0.5}Ga_{0.5}As$ monolayers at the interfaces [(b) and (c)]. The vertical lines mark the peaks plotted in Fig. 6. Lower panels: local density of longitudinal states at $\mathbf{q}=(0,0,q_z\rightarrow 0)$ on the cationic planes of the superlattice unit cell. The composition of the layers is indicated on the left side of each panel.

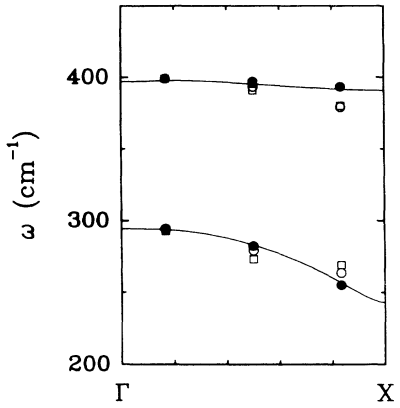

FIG. 6. "Unfolding" of calculated Raman-active superlattice frequencies [$z(xy)\bar{z}$ configuration] onto the theoretical bulk dispersions (solid lines). Full circles: ideal $(GaAs)_5(AlAs)_5$ (001) superlattice [see Fig. 5(a)]; open circles (squares): the same superlattice, but with one (two) intermixed $Al_{0.5}Ga_{0.5}As$ layers at the interfaces [see Figs. 5(b) and 5(c)]. Compare with the experimental data of Fig. 1.

currence of cationic disorder at the interface is responsible for the discrepancies between existing experimental data and previous calculations.

Our results show that cationic intermixing tends to lower the frequencies of Raman-active peaks, except for GaAs-like modes with effective wave vectors near the zone boundary, the deviations of the peak positions with respect to ideal SL's being larger in the AlAs than in the GaAs range. Unfolding the SL modes by the same procedure as in ideal SL's (as it is done in Fig. 1, where disorder effects are not even considered) relies on the assumption that the observed modes of the intermixed structures can still be considered as confined in the $(GaAs)_5$ or the $(AlAs)_5$ layers. As it will be evident below, this assumption is quite groundless. A careful analysis of our theoretical results allows one to understand the origin of the individual Raman peaks and to explain the different behavior of GaAs-like and AlAs-like structures. The lower panels of Fig. 5 show the longitudinal density of states (LDOS) locally projected onto the different cationic planes in the ideal and in the model disordered configurations. Let us first examine the ideal case: five LO-confined GaAs- and AlAs-like modes exist, giving rise to five peaks in the LDOS, which are well separated in the GaAs-like range, and very close in the AlAs-like one [due to the flatness of the AlAs LO dispersion along (001)]. Out of these, only those with even parity—which can be recognized by the finite LDOS amplitude in the central plane of each slab—contribute to the Raman intensity in the scattering configuration we are considering.

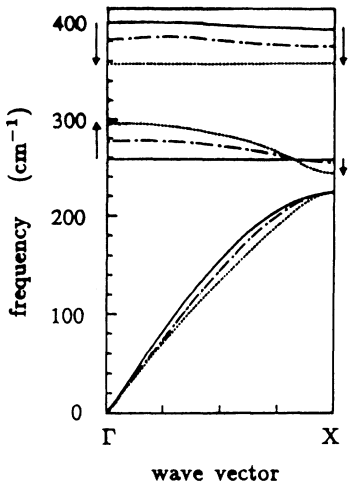

FIG. 7. Phonon dispersions of GaAs-like and AlAs-like L modes of $Al_xGa_{1-x}As$ along the Γ-X direction, at $x=0$ (dotted lines), $x=0.5$ (dashed-dotted lines), and $x=1$ (solid lines). The horizontal lines in the GaAs (AlAs)-like frequency range for $x=1$ ($x=0$) represent the frequency of the isolated Al (Ga) impurity in GaAs (AlAs). The arrows mark the sign of the frequency variation at Γ and X with decreasing x: note the quasirigid shift of the AlAs-like branch; note also the opposite sign of the Γ and X shifts of the GaAs-like branch (see Ref. 11).

The Raman spectrum is dramatically modified by a mixed layer at the interfaces, particularly in the AlAs-like frequency range: inspection of the LDOS reveals that the additional peak arising at low frequencies (~ 380 cm^{-1}) does *not* correspond to a confined state extending all over the AlAs slab but, rather, it clearly originates from the alloyed layer; indeed, its frequency is slightly lower than the frequency of the bulk alloy [calculated in Ref. 11 with the same technique (see Fig. 7)] owing to confinement over a single layer. The remaining peaks shift to the positions appropriate to confinement in a four-layer region. This behavior derives from the smallness of the AlAs-like phonon bandwidth of $Al_xGa_{1-x}As$, as compared to the dependence of its absolute position upon composition: as a consequence, the alloy band is well separated from the bulk AlAs band already for Al concentrations as high as 90–95 %.[14]

The situation is more complex in the GaAs-like frequency range, where the alloy and bulk bands partially overlap.[11,15] The effect of alloying is to narrow the LO band and to shift it to lower frequencies. For frequencies above the overlap region, vibrations (which are characterized by a small wave vector) can only propagate in the pure-GaAs slab and cannot penetrate into the disordered region. Their confinement length is therefore reduced from five to four layers, the wave vector increased, and the corresponding quantized frequency reduced accordingly. This behavior is clearly demonstrated in Fig. 5(b) which indicates that the first two modes with higher frequency (one active, one inactive) are confined over four cationic planes. In the overlap range (which corresponds to lower frequencies and to larger wave vectors) LO vibrations of the GaAs slab also extend to the alloyed interface region; the effective confinement is increased accordingly, and the frequency raised. This is also confirmed by Fig. 5(b): the lowest-lying mode extends over six cationic planes and is inactive ($m=6, n=6$). The following one in order of increasing frequency also extends over six cat-

ionic planes and is Raman active ($m=5, n=6$). The remaining Raman-active mode has an intermediate behavior: it extends mainly over four cationic planes, but it also has some amplitude over the two remaining (alloyed) planes. More results for different Al contents in the intermixed layer will be presented in Sec. IV.

B. Problem 2: thickness dependence of optical frequencies in ultrathin SL's

To study the effect of intermixing in ultrathin $(GaAs)_n/(AlAs)_n$ structures we first consider a set of $(Al_xGa_{1-x}As)_n(Al_{1-x}Ga_xAs)_n$ SL's, whose average Al composition is 0.5. The results for the highest Raman-active frequencies are shown in Fig. 8 for different values of x. The most prominent feature is that all the GaAs (AlAs)-like peaks undergo large shifts to lower frequencies when the maximum Ga (Al) concentration is decreased, except for the GaAs-like peak at $n=1$, which moves slightly upwards.

Inspection of Fig. 7 provides insight also into this feature. In fact, AlAs-like bands in the bulk alloy shift almost rigidly toward lower frequencies when the Ga concentration increases: this implies that the AlAs-like modes in SL's are pushed down by intermixing, independently of their wave vector. Instead, GaAs-like modes in the bulk alloy are shifted *down* by increasing the Al concentration only for wave vectors $q \leq q_c \approx (3\pi)/(2a)$. Beyond this critical wave vector (whose value is roughly independent of composition), LO modes are instead pulled *up*. It follows that the GaAs-like SL modes whose confinement wave vector is smaller than q_c are pushed down by cationic intermixing. The only mode which has a sizable zone-border character [$q \gtrsim (3\pi)/(2a)$] is that of the monolayer SL ($n=1$), which is, in fact, the only one pulled up by disorder.

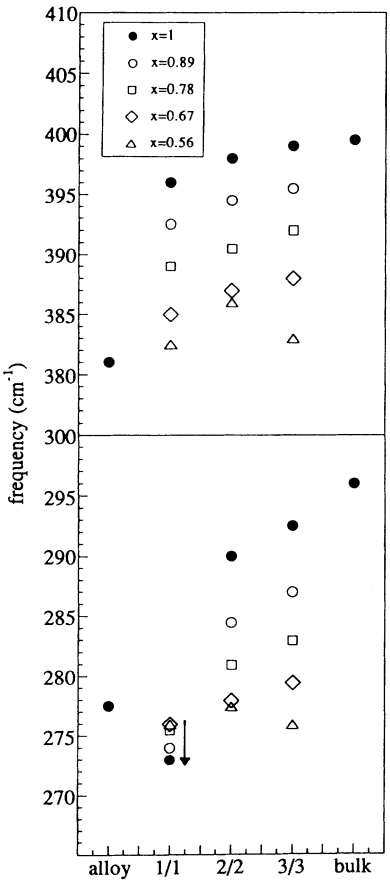

FIG. 8. Highest Raman-active peaks calculated for ultrathin $(Al_xGa_{1-x}As)_n(Ga_xAl_{1-x}As)_n$ (001) superlattices, with $n=1,2,3$. Full circles: $x=1$, i.e., ideal $(GaAs)_n(AlAs)_n$ superlattices; empty circles: $x=0.89$; squares: $x=0.78$; diamonds: $x=0.67$; triangles: $x=0.56$. The "alloy" values refers to $Al_{0.5}Ga_{0.5}As$ and are from Ref. 11. The arrow marks the frequency variation with varying composition for GaAs-like ω_{LO_1} in the $n=1$ superlattice. Note that its sign is opposite to all the other cases.

For the monolayer SL, the choice of the $(Al_xGa_{1-x}As)_1(Al_{1-x}Ga_xAs)_1$ configuration involves no assumption except in-plane homogeneity. For $n=2$ and 3, instead, the (homogeneous alloy)-(homogeneous alloy) configuration is certainly not the best description of cationic intermixing in actual samples; however, at a given value of x, it gives, in general, a *lower limit* for the shift of ω_{LO_1} which can appear in SL's where the purest AlAs (GaAs) planes have x concentration. Indeed, a cationic distribution which is less homogeneous along z increases such deviation by further confining the vibrational amplitudes associated with those frequencies. This is confirmed by the example of Fig. 9, where the results of Fig. 8 for the $n=2$ SL are compared with more inhomogeneous configurations.

Our results of Fig. 8 are therefore a good starting point for a comparison with the experimental results of Fig. 2.

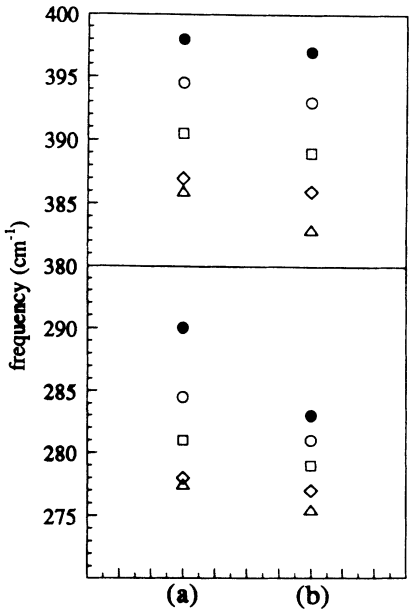

FIG. 9. Example of the effect of cationic intermixing on ultrathin superlattices having the same periodicity and average concentration, but different distributions of cations: (a) $(Al_xGa_{1-x}As)_2(Ga_xAl_{1-x}As)_2$; (b) $(Al_{0.5}Ga_{0.5}As)_1(Al_xGa_{1-x}As)_1(Al_{0.5}Ga_{0.5}As)_1(Ga_xAl_{1-x}As)_1$. The symbols correspond to the same values of x as in Fig. 8.

In the GaAs-like range, we note that the opposite sign of the disorder-induced frequency shift for $n=1$ with respect to $n=2$ and 3 is the key feature allowing us to explain the smooth dependence upon n observed in the experimental data. Quantitatively, for $n=1$ a very large deviation of x from the ideal value $x=1$ must be present, in order to account for the peak position measured for the samples of Fig. 2. For $n>1$, some degree of intermixing, such that the *purest* planes have $x=0.75-0.85$ for $n=2$ and $x=0.85-1$ for $n=3$, would give an n dependence in agreement with the experimental data of Fig. 2.

IV. AlAs-LIKE SUPERLATTICE MODES AS FINGERPRINTS FOR CHARACTERIZATION

The purpose of this section is to show how the dependence upon composition of AlAs-like LO modes in $Al_xGa_{1-x}As$ bulk alloys, together with the flatness of the corresponding band along (001), can provide accurate and detailed information for characterizing the quality of superlattices. Consider, for instance, a SL in which two adjacent cationic planes have different Al concentrations, such that the corresponding bulk-alloy AlAs-like frequencies differ more than the LO bandwidth: it is clear that in this case AlAs-like vibrations will be confined over individual planes, and that their frequencies will provide a direct measure of the corresponding composition. In practice, AlAs-like LO vibrations are confined over one individual cationic plane whenever the composition difference between neighboring cationic planes is large enough that Raman-active modes in the bulk alloys at the two compositions differ by more than $\sim 3-4\ cm^{-1}$. This idea can provide *quantitative* information about the composition profile resulting from disorder which unintentionally occurs during epitaxial growth. To show this, we will consider two prototypical situations: the first—which is also the object of recent experimental investigations[16,17]—consists of an isolated $Al_xGa_{1-x}As$ monolayer embedded between two thicker GaAs layers; the second consists of a monolayer of $Al_xGa_{1-x}As$ at the interface between GaAs and AlAs (this configuration has already been considered in Sec. III for the special case $x=0.5$).

In both cases we find that the alloy layer gives rise to well-defined AlAs-like peaks in the Raman spectra, which, in a wide range of compositions, are well separated in frequency from any other SL peak. Moreover, we find that the frequencies of these peaks depend sensitively and quasilinearly upon x, and, therefore, can be easily used as a measure of the local composition.

A. One monolayer of $Al_xGa_{1-x}As$ in GaAs

We start by considering an ideal $(GaAs)_5(AlAs)_1$ SL, for which the calculated $z(xy)\bar{z}$ Raman spectrum is shown in the top panel of Fig. 10. The AlAs monolayer

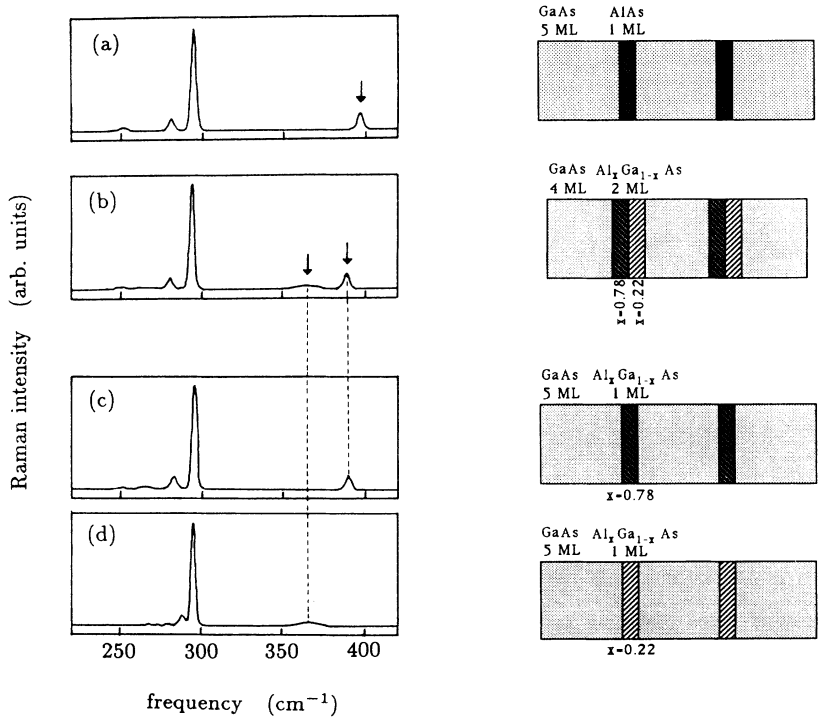

FIG. 10. Calculated Raman intensity profiles in the $z(xy)\bar{z}$ configuration for the (001) superlattices sketched on the right-hand side: (a) ideal $(GaAs)_5(AlAs)_1$ superlattice; (b) $(GaAs)_4(Al_{0.78}Ga_{0.22}As)_1(Al_{0.22}Ga_{0.78}As)_1$, having the same period and average concentration as (a), but with the Al content distributed over 2 monolayers. (c) and (d) are reference $(GaAs)_5(Al_xGa_{1-x}As)_1$ structures with $x=0.78$ and $x=0.22$, respectively. The arrows in (a) and (b) mark the AlAs-like peaks of interest for characterization.

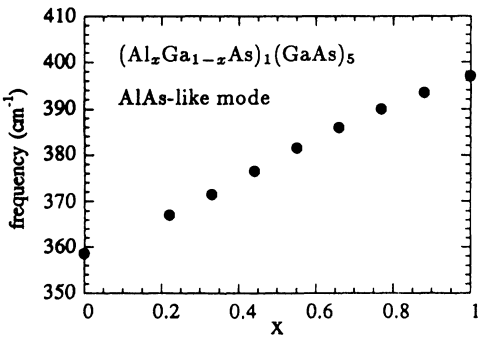

FIG. 11. Composition dependence of the frequency of the AlAs-like mode in a $(GaAs)_5(Al_xGa_{1-x}As)_1$ superlattice.

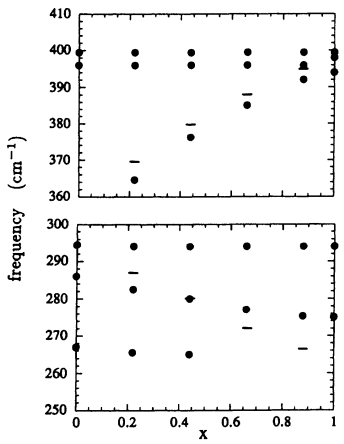

FIG. 12. Composition dependence of the frequency of the AlAs-like and GaAs-like modes (top and bottom panels, respectively) in a $(GaAs)_4$ $(Al_xGa_{1-x}As)_1(AlAs)_4$ $(Al_xGa_{1-x}As)_1$ superlattice. The LO frequencies of the $Al_xGa_{1-x}As$ bulk alloy are shown by horizontal ticks as a reference.

gives rise to a confined mode in the AlAs-like range. Moreover, it is able to act as an effective barrier for GaAs vibrations. In fact, three distinct Raman-active GaAs-like peaks are present (ω_{LO_1}, ω_{LO_3}, and ω_{LO_5}), whose frequencies are only very slightly modified with respect to the case of thicker barriers [compare with $(GaAs)_5(AlAs)_5$ in Fig. 5].

We will now show that the study of AlAs-like Raman peaks allows one to discriminate between the ideal configuration (one sharp AlAs monolayer with no intermixing) and the situation where the Al content is spread over two monolayers with different concentrations. The second panel of Fig. 10 displays the calculated spectrum when such concentrations are chosen to be 0.78 and 0.22. Two peaks appear instead of one, both clearly shifted to lower frequency with respect to the ideal configuration. For a better illustration of their origin, in the lower part of the same figure we also report the spectra obtained for the isolated monolayers with $x=0.78$ and 0.22. In the AlAs frequency range, the spectrum of Fig. 10(b) is an almost perfect superposition of those of Figs. 10(c) and 10(d). Furthermore, the frequency of these peaks gives a very clear indication of the Ga concentration of the mixed layers. Figure 11 presents the x dependence of the AlAs-like frequency for $(GaAs)_5(Al_xGa_{1-x}As)_1$. The trend between the values at the two extrema (corresponding to a pure AlAs monolayer at $x=1$ and to the isolated Al impurity in GaAs at $x=0$) is almost linear. A more complete discussion of these results and their relevance to recent experimental data[16] will be presented elsewhere.[17]

B. Quantitative estimates of interdiffusion at interfaces

The existence of a well-defined AlAs-like peak arising from the interdiffused region in the GaAs/AlAs SL of Fig. 5(b) suggests that the frequency of such a peak can be used as a measure of the corresponding Al concentration, as done in the previous section for the individual AlAs monolayer in GaAs. To verify this possibility, we have studied a $(GaAs)_4(Al_xGa_{1-x}As)_1(AlAs)_4(Al_xGa_{1-x}As)_1$ SL at different values of x. The frequencies of the Raman-active peaks are plotted versus x in Fig. 12, together with results of ideal $(GaAs)_6(AlAs)_4$ and $(GaAs)_4(AlAs)_6$ SL's which correspond to the extreme values $x=0$ and 1, respectively. The upper edge of the bulk alloy bands are also plotted as a reference.

A very different behavior characterizes the two frequency regions of Fig. 12. In the AlAs-like range, the two highest peaks (ω_{LO_1} and ω_{LO_3}) are almost independent of x except for the largest x values, while the lowest peak follows the quasilinear x dependence typical of the bulk $Al_xGa_{1-x}As$ alloy. Again, this is a consequence of the fact that the AlAs-like band of pure AlAs [and, therefore, the modes confined in the $(AlAs)_4$ layer] never overlaps the AlAs-like band of the alloy except for the largest x values. In the GaAs-like range, instead, the vibrations of the pure GaAs layer may overlap in frequency with the alloy band, thus modifying their effective confinement length. Only the higher mode, ω_{LO_1}, falls out of the alloy band at all concentrations; for ω_{LO_3} this is true only for $x>0.5$. Therefore, ω_{LO_1} does not depend on x except for very small concentrations (a small jump is indeed visible in Fig. 12 between $x=0$ and $x=0.2$), while ω_{LO_3} approaches the value corresponding to confinement in six (four) monolayers as x approaches its lowest (highest) extreme. The variation of each GaAs-like mode with x, therefore, depends on its frequency relative to the alloy band, and in general can be estimated only from a detailed calculation. On the other hand, if an AlAs-like peak is detected outside the bandwidth allowed for pure AlAs, its frequency can be taken as a measure of the Al concentration in the intermixed layer.

V. CONCLUSIONS

In summary, we have shown that a theoretical approach, based on first-principles *interatomic* force constants calculated via density-functional perturbation

theory, allows one to perform accurate calculations of phonon dispersions and displacements in systems with a large number of atoms in the unit cell, and to study ideal as well as compositionally disordered GaAs/AlAs superlattices.

The results clearly indicate the role of cationic intermixing in determining both the thickness dependence of the highest Raman peaks in ultrathin superlattices as well as the position and intensity of "high-order" Raman peaks in thicker superlattices, thus solving two long-standing problems in the interpretation of Raman spectra. We conclude that short-range compositional disorder close to the interfaces is never negligible, at least in samples grown by molecular-beam epitaxy at the usual substrate temperatures.[18,19]

Raman-active modes—particularly the AlAs-like ones—are found to be very sensitive to compositional disorder and, therefore, suitable for a quantitative characterization of cationic intermixing. The study of phonons as local probes of the crystal structure appears to be an important tool which may contribute to the present debate[20] on the microscopic structure of GaAs/AlAs interfaces.

ACKNOWLEDGMENTS

We are grateful to A. Fasolino, B. Jusserand, and J. Menéndez for many useful discussions. This work was supported in part by CNR under Grants No. 90.00653.PF69 (S.B.) and No. 90.00658.PF69 (E.M.) and by the Swiss National Science Foundation under Grant No. 20-5446.87 (P.G. and S.d.G.). S.B. also acknowledges partial support by the European Research Office of the U.S. Army under Grant No. DAJA 45-89-C-0025.

---

*Permanent address: Scuola Internazionale Superiore di Studi Avanzati (SISSA), via Beirut 4, I-34014 Trieste, Italy.

[1]For recent reviews, see: (a) B. Jusserand and M. Cardona, in *Light Scattering in Solids V,* edited by M. Cardona and G. Güntherodt (Springer, Berlin, 1989), p. 49; (b) J. Menéndez, J. Lumin. **44**, 285 (1989); (c) A. Fasolino and E. Molinari, Surf. Sci. **228**, 112 (1990).

[2]A. K. Sood, J. Menéndez, M. Cardona, and K. Ploog, Phys. Rev. Lett. **54**, 2111 (1985).

[3]B. Jusserand and D. Paquet, Phys. Rev. Lett. **56**, 1753 (1986).

[4]E. Molinari, A. Fasolino, and K. Kunc, in *Proceedings of the 18th International Conference on the Physics of Semiconductors, Stockholm, Sweden, 1986,* edited by O. Engström (World Scientific, Singapore, 1987), p. 663; Superlatt. Microstruct. **2**, 397 (1986).

[5]G. Fasol, M. Tanaka, H. Sakaki, and Y. Horikoshi, Phys. Rev. B **38**, 6056 (1988).

[6]Z. P. Wang, D. S. Jiang, and K. Ploog, Solid State Commun. **65**, 661 (1988).

[7]D. J. Mowbray, M. Cardona, and K. Ploog, Phys. Rev. B **43**, 1598 (1991).

[8](a) M. Cardona, T. Suemoto, N. E. Christensen, T. Isu, and K. Ploog, Phys. Rev. B **36**, 5906 (1987); (b) A. Ishibashi, M. Itabashi, Y. Mori, K. Kawado, and N. Watanabe, *ibid.* **33**, 2887 (1986); (c) M. Nakayama, K. Kubota, and N. Sano, Solid State Commun. **53**, 493 (1985); (d) T. Toriyama, N. Kobayashi, and Y. Horikoshi, Jpn. J. Appl. Phys. **25**, 1895 (1986).

[9]S. Baroni, P. Giannozzi, and E. Molinari, Phys. Rev. B **41**, 3870 (1990).

[10]A partial account of the present results was presented by E. Molinari, S. Baroni, P. Giannozzi, and S. de Gironcoli, in *Proceedings of the 20th International Conference on the Physics of Semiconductors, Thessaloniki, Greece, 1990,* edited by E. Anastassakis and J. D. Joannopoulos (World Scientific, Singapore, 1990), p. 1427; Appl. Surf. Sci. (to be published).

[11]S. Baroni, S. de Gironcoli, and P. Giannozzi, Phys. Rev. Lett. **65**, 84 (1990).

[12]P. Giannozzi, S. de Gironcoli, P. Pavone, and S. Baroni, Phys. Rev. B **43**, 7231 (1991).

[13]The Raman cross section is calculated by ignoring any differences between Ga and Al polarizabilities, as explained in Ref. 11.

[14]The existence of well-defined frequency-versus-wave vector phonon dispersions in $Al_xGa_{1-x}As$ alloys is revealed and discussed in Refs. 15 and 11.

[15]B. Jusserand, D. Paquet, and F. Mollot, Phys. Rev. Lett. **63**, 2397 (1989).

[16]B. Jusserand, in *Light Scattering in Semiconductor Structures and Superlattices,* edited by D. J. Lockwood and J.F. Young (Plenum, New York, 1991), p. 39; B. Jusserand, in *Proccedings of the 20th International Conference on the Physics of Semiconductors, Thessaloniki, Greece, 1990,* edited by E. Anastassakis and J. D. Joannopoulos (World Scientific, Singapore, 1990), p. 1985.

[17]B. Jusserand, F. Mollot, E. Molinari, and S. Baroni, in *Proceedings of the 5th International Conference on Modulated Semiconductor Structures, Nara, 1991* [Surf. Sci. (to be published)]; and (unpublished).

[18]The effect of different growth temperatures on cationic intermixing—as studied by Raman scattering—is discussed in Ref. 17.

[19]J. Grant, J. Menéndez, L. N. Pfeiffer, K. W. West, E. Molinari, and S. Baroni, Appl. Phys. Lett. **59**, 2859 (1991).

[20]See, e.g., B. Deveaud, B. Guenais, A. Poudoulec, A. Regreny, and C. d'Anterroches, Phys. Rev. Lett. **65**, 2317 (1990); A. Ourmazd and J. Cunningham, Phys. Rev. Lett. **65**, 2318 (1990), and references therein.

[21]D. Strauch and B. Dorner, J. Phys. Condens. Matter **2**, 1457 (1990).

[22]A. Onton, *Proceedings of the 10th International Conferences on the Physics of Semiconductors,* edited by S. P. Keller, J. C. Heusel, and F. Stern (U.S. Atomic Energy Commission, New York, 1970), p. 107; B. Monemar, Phys. Rev. B **8**, 5711 (1973).

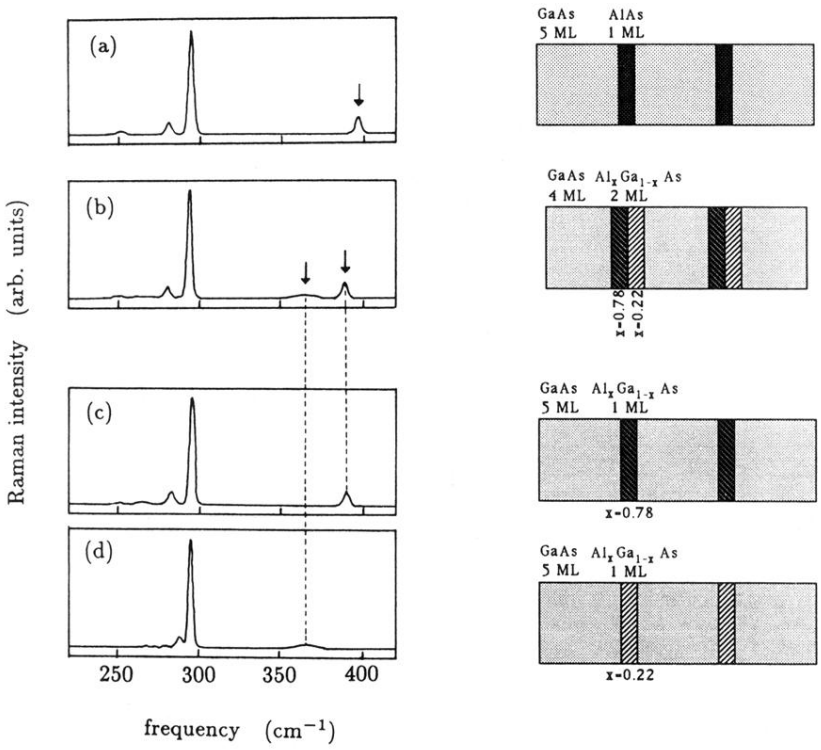

FIG. 10. Calculated Raman intensity profiles in the $z(xy)\bar{z}$ configuration for the (001) superlattices sketched on the right-hand side: (a) ideal $(GaAs)_5(AlAs)_1$ superlattice; (b) $(GaAs)_4(Al_{0.78}Ga_{0.22}As)_1(Al_{0.22}Ga_{0.78}As)_1$, having the same period and average concentration as (a), but with the Al content distributed over 2 monolayers. (c) and (d) are reference $(GaAs)_5(Al_xGa_{1-x}As)_1$ structures with $x=0.78$ and $x=0.22$, respectively. The arrows in (a) and (b) mark the AlAs-like peaks of interest for characterization.